# NUMERICAL STUDIES RELATED TO THE DESIGN OF THE BEAM TARGET OF THE ENERGY AMPLIFIER PROTOTYPE

S. Buono, V. Bellucci, G. Fotia, L. Maciocco, V. Moreau, M. Mulas, G. Siddi, L. Sorrentino

CRS4 Research Centre - Via N. Sauro 10 - 09123 Cagliari, Italy

***Abstract***

*The Centre for Advanced Studies, Research and Development in Sardinia (CRS4) is participating in an Italian R&D program, together with Ansaldo, ENEA and INFN, devoted to the design of a 80 MW prototype of the Energy Amplifier proposed by C. Rubbia et al.. The use of advanced numerical tools has been of practical support in the design of critical elements of the machine such as the fuel element and the beam target.*

*The aim of this work is to show the design and optimization of the Liquid Metal Spallation Target, which consists in an axial-symmetric vertical cylinder, where a Pb-Bi eutectic, in a natural convection driven flow regime, works at the same time as spallation material and coolant for the target and the beam window. The most critical part of the target is the window itself, where the highest temperatures and thermal stresses are reached. The minimization of such temperatures and stresses is the goal of the optimization.*

*The main geometrical dimensions of the target (i.e. beam pipe, beam window and external container) are somehow fixed since they are related to the proton beam distribution and to the EA core design. The optimization therefore acts on the suitable design of the flow guide which separates the hot rising flow from the cold one. In the region where the flow is heated by the proton beam the flow guide has a funnel shape which accelerates the liquid metal.*

*The numerical simulations are performed by using three different tools. The FLUKA Montecarlo code is used to calculate the heat source distribution in the window and in the coolant generated by the interaction with the proton beam. The results of these calculations are used as input data for the thermal fluid dynamic simulations performed with the STAR-CD commercial software. The resulting temperature and pressure fields are finally introduced in the NASTRAN code used for the structural analysis of the solid components.*

## Introduction

The function of the beam target is the one of supplying an external source of neutrons to the subcritical core of the Energy Amplifier [1] (EA). Neutrons come from the interaction of a high power proton beam with a high A medium (the target material). Such interaction, called spallation, has the undesirable effect of (1) producing a large quantity of heat (typically some MW) concentrated in a small volume, which has to be removed, and (2) inducing an intense radiation damage in the structural materials. The target represents one of the main technological problems related not only to the design of an EA Prototype (EAP), but to all High Power Spallation Sources (HPSS) currently under study or in construction world-wide [2, 3].

## Target physics

The spallation interaction is very efficient in producing neutrons for proton energies higher than 1 GeV [4]. The beam energy is amplified by the subcritical core according to the formula

$$P = P_0 \cdot \frac{G_0}{1 - k_s}$$

Paper presented to the International Workshop on ≥Heavy Liquid Metal Coolants in Nuclear Technology≤, IPPE, Obninsk, Russia, October 5-9, 1998

where P is the thermal power of the machine, $P_0$ is the beam power, $G_0$ is a gain factor, which is a function of the beam energy and the characteristics of the target, and $k_s$ is the neutron multiplication coefficient of the sub-critical system. For a beam energy of 600 MeV, as it is foreseen for the EAP, $G_0$ is about 1.5, which implies a beam power ranging from 1 to 3.7 MW for a nominal $k_s$ of 0.98 to 0.93 and a total power of 80 MW. The beam power is related to the beam current and the beam energy according to the formula

$$I(mA) = \frac{P_0(MW)}{E(GeV)}$$

The accelerator current during the EAP lifetime, will therefore range from about 2 to 6 mA. The beam size is assumed to be a circular spot of $r_0$ = 7.5 cm radius, with the proton intensity distributed as the paraboloid:

$$\frac{2I_o}{\pi r_o^2}\left(1-\frac{r^2}{r_o^2}\right)$$

where $I_0$ is the beam current. The reasons of such a defocused beam have to be found in the necessity of reducing the power densities in the target which, as shown in figure 1 according to a Fluka [5] calculation, reach considerable values and require a very effective cooling of the system.

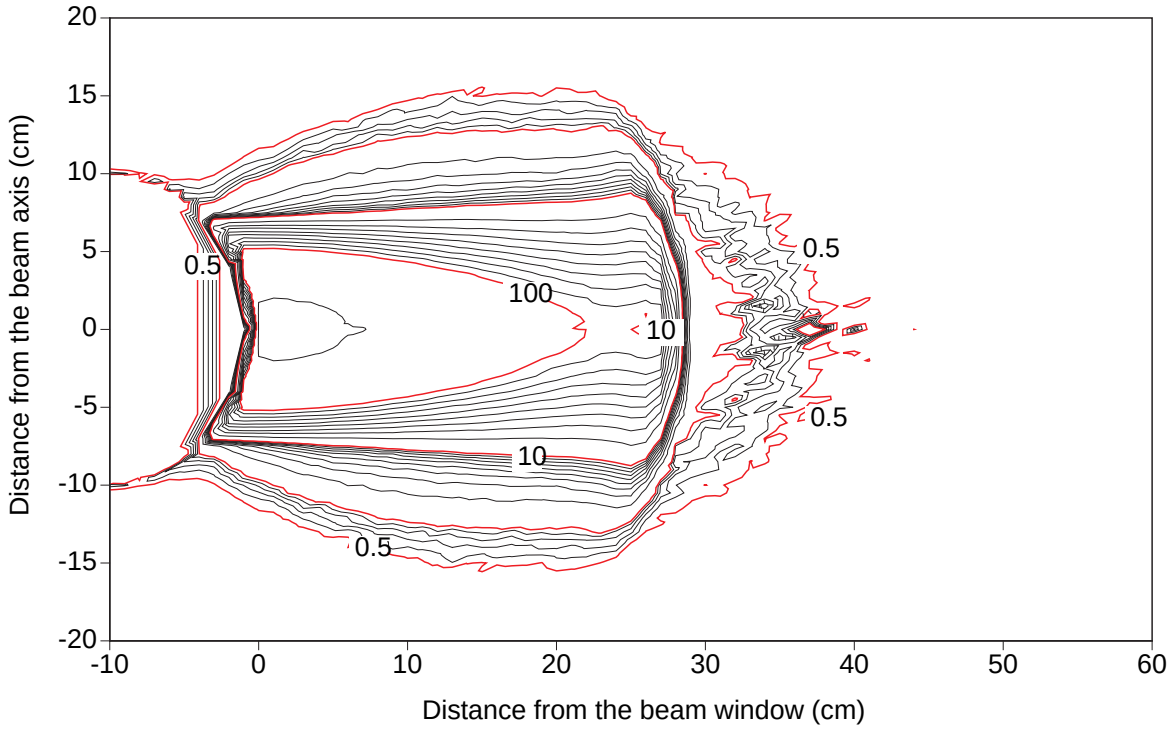


***Figure 1.*** *Power generated by a 600 MeV proton beam in a thick Lead-Bismuth target. Units are in* $W/cm^3/mA$

Nevertheless, not all the power contained in the beam is deposited in the spallation target [6]. In the case of a 600 MeV proton beam, for example, the energy deposited in form of heat is about 72 %, the rest being contained in the particles escaping the system or in the binding energy of the target nucleus.

### Target material

Liquid metals satisfy the important criteria of being the spallation medium and the cooling fluid at the same time and are currently considered the best choice in terms of target materials [2,3] since their structural and thermal properties are not degraded by the radiation damage induced by proton interactions. Given the fact that the primary

cooling loop of the EAP is made of Lead Bismuth Eutectic (LBE), we considered the same material for the beam target.

**Beam window**

The most common target configurations adopted in HPSS designs include a beam window which separates the internal vacuum of the beam pipe from the molten metal target. The most important problems related to all target designs are (1) target cooling, (2) high energy neutron radiation damage and (3) liquid metal corrosion. Configurations using a beam window have the additional problems of the beam window cooling and the radiation damage induced in the beam window material, which is of a slight different nature of the one induced in the other structures, since the window is exposed not only to back scattered high energy neutrons, but also to the high energy proton flux.

The proton beam can deposit in the window up to 3 % of its energy, depending on the materials used in the window, its geometry and the beam energy and dimension. This means many tens of kWatts, concentrated in a small volume. The choice of the beam window material is therefore very delicate and depends on many factors (physical and structural properties, activation properties, working temperature, compatibility with liquid Pb-Bi environment) which are often not independent one on another. An ideal material should have the following characteristics:

Low density.

High thermal conductivity.

Low thermal expansion coefficient.

Low Young Modulus.

Small Poisson's ratio.

High tensile strength.

Low DBTT (Ductile to Brittle Transition Temperature) under radiation exposure.

High corrosion resistance to liquid metal exposure.

High resistance to proton induced radiation damage.

All these characteristics are strongly dependent on the temperature and show different tendencies. For example tensile strength and corrosion resistance decrease drastically with the increase in temperature, while in general radiation damage resistance and brittle behavior improve. It is clear that for each material there is an ideal operating temperature (or a range of temperatures) which enhances the lifetime of the window. In reference [7] we defined the *Window efficiency* as a useful parameter to understand the delicate interplay of the physical and mechanical properties of materials at different operating temperatures.

Unfortunately at the present moment no sufficient experimental data are available on the behavior of structural materials under the combined effect of intense proton irradiation and liquid metal exposure. Main concerns are related to H or He swelling (production rate will be much higher than in a reactor environment due for example to (p, $\alpha$), (p, p) or high energy (n, $\alpha$), (n, p) reactions) and liquid metal embrittlement. Other effects such as irradiation hardening or irradiation creep can also have unexpected behaviors due to a harder spectrum, compared with traditional reactor environments. Transmutation of beam window materials into foreign elements can also have a negative effect due to the formation and precipitation of impurities.

It is therefore extremely difficult to predict the lifetime of this object which could be even lower of the one of a common fuel cladding material. The EAP design has therefore to include the possibility of a rapid replacement of the beam window. While steels might be suitable candidates for low power applications [2,3], refractory alloys or more advanced materials are mandatory for high power applications [7, 8].

**Geometry**

The target region has to fit in the central hole of the sub critical core which has currently a free diameter of about 55 cm. Beam penetration must occur from the top of the vessel, for obvious reasons (necessity of maintaining the integrity of the vessel to prevent coolant losses). The target region above the core has the same maximum diameter in order to be compatible with the fuel loading machine operations.

The coolant has therefore to be injected from the top, reaches the interaction region where it heats up and returns again to the top of the EAP vessel. Considering the slim geometry of the system it is advisable that the flow directions follow the sense of the natural convection (hot Pb-Bi rising, cold Pb-Bi descending). In this way the pumping mechanism will be strongly reduced if not suppressed, in the case natural convection alone was enough to cool the beam window.

The target geometry is described in figure 2. It is an axial symmetric device consisting of a vertical pipe (*beam pipe*) closed at the bottom by an hemisphere of variable thickness (*window*); the beam pipe is enclosed in a vertical coaxial cylinder with an hemispherical bottom (*container*). The region between the beam pipe and the container is filled with the spallation/cooling fluid (*coolant*). The region inside the beam pipe is void.The coolant flow is guided by a coaxial cylinder laying between the beam pipe and the container (*flow guide*) which separates the hot rising flow coming from the spallation region from the cold down coming flow cooled in the heat exchanger, which is positioned on the top of the down coming duct. In the spallation region the flow guide is shaped like a funnel in order to enhance the cooling of the window. The funnel is made of a converging duct (*inducer*), which turns the flow from the down coming duct into the short pipe (*funnel*) where the spallation takes place. The funnel and the rising duct are connected by a divergent duct (*connector*).

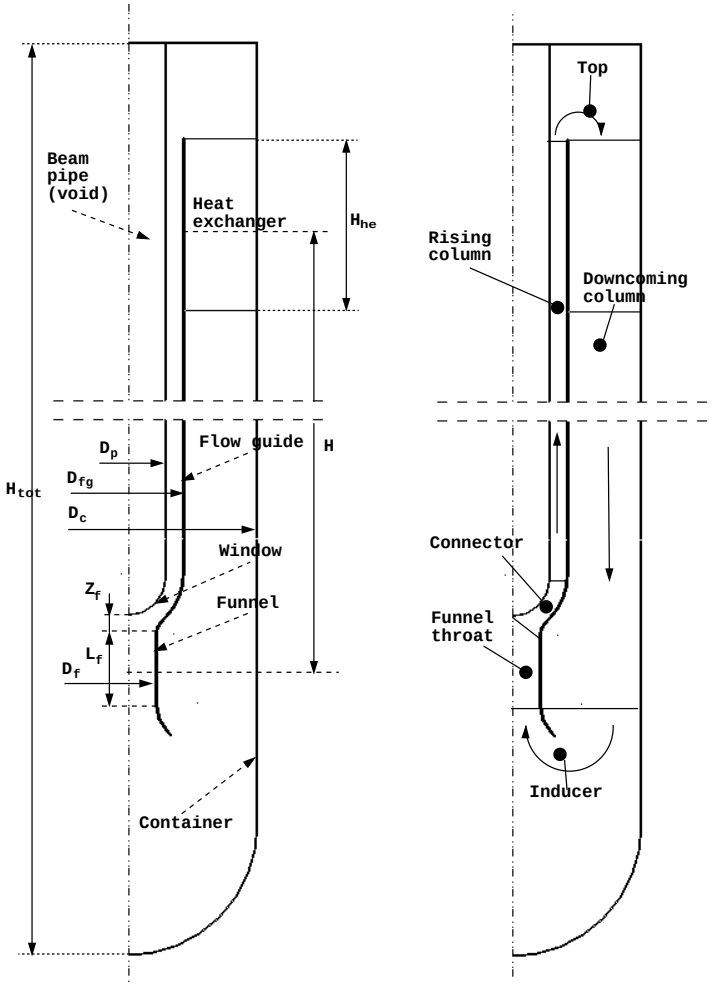


***Figure 2.*** *Target geometry*

The beam pipe diameter is 20 cm, in order to allow a correct defocusing of the beam spot to prevent localized high power density in the target materials. The external surface of the window is a hemisphere while the internal surface is an ellipsoid, so that the window thickness varies from a minimum of 1.5 mm in the beam axis to a maximum of 3 mm in the junction with the beam pipe; this was done in order to reduce as much as possible the thickness in the zone where proton irradiation is higher, keeping a sufficient structural resistance. The beam pipe and the container are made of HT-9 steel. Regarding the beam window material, in reference [1] we proposed the

use of a Tungsten alloy for the Energy Amplifier. In this study we considered also the use of a conventional ferritic steel (HT9), given the much lower thermal power of the prototype. The choice will be justified by a comparison of the respective performances.

## The numerical model

The turbulent incompressible flow of the Pb-Bi in the target has been simulated using the Star-CD commercial code [9]. The equations for the conductive heat transfer across the solid regions are solved coupled with the fluid dynamic equations. Second order schemes are employed for the spatial discretization. Turbulence is modeled with a Chen k-ε using a two-layer algorithm in the near wall region.

We used the IDEAS CAD [10] to create a parametric mixed structured/unstructured mesh. Unstructured meshes are used in zones with irregular geometry and whose shape varies with the values of the parameters as it is sown in figure 3 for the funnel zone. The fluid regions near the walls are meshed with structured grids, easier to handle and more suitable for the application of the turbulent near-wall algorithms.

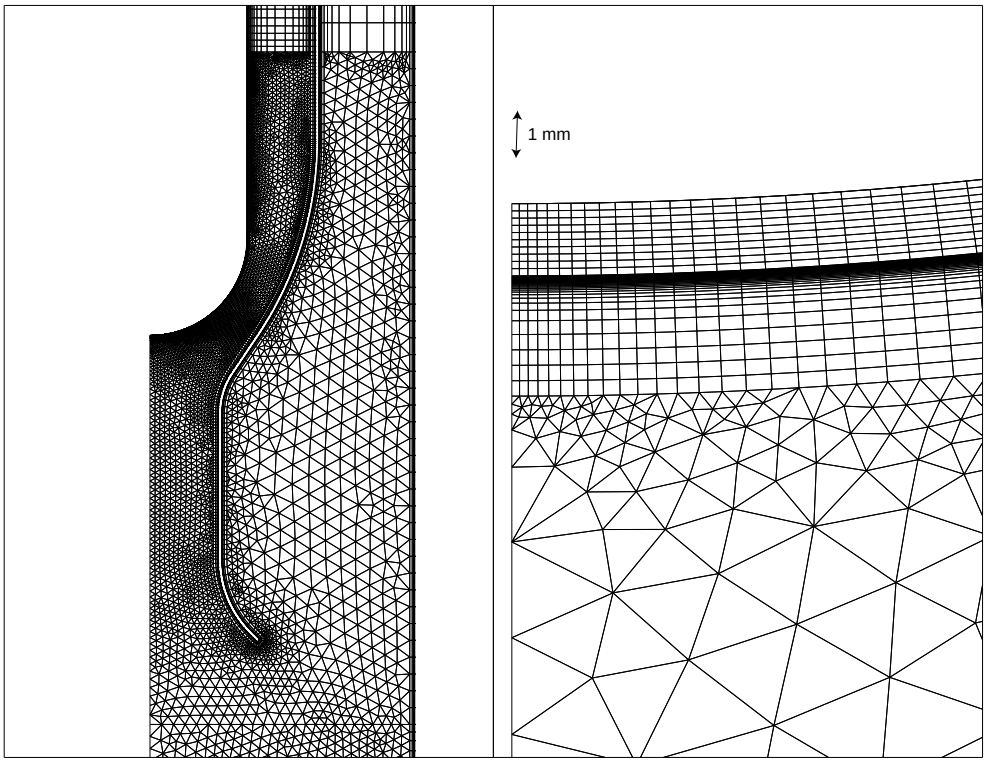


***Figure 3.*** *Details of the Target mesh*

Structured meshes are also used for the discretization of the solids. The flow guide is split into three regions along its thickness to allow the simulation of an insulation. In order to make possible the use of meshes with different coarseness in the rising and down coming sides, the flow guide is discretized with a non-conform mesh. The total number of cells is about 25000 (it varies while changing the parameters in the non structured zones). The discretization is very accurate in the funnel zone, especially next to the window stagnation point as it is shown in figure 3. Cells with high aspect ratio are used in the rising and down coming duct, where the flow is supposed to be regular.

The same grid used for the Thermal Fluid Dynamic simulation was employed for the finite element structural analysis of the beam pipe/window system performed with NASTRAN [11]. The nodes belonging to the beam pipe upper surface have been constrained with a slider that restrains the displacements normal to the plane of that surface. The choice of this constraint is not relevant because its effects are quickly damped in the very vicinity of

the constraint itself. The temperature field calculated by Star-CD is assigned to the elements of the model and the Pb-Bi hydrostatic pressure distribution is applied onto the external surface.

**Window material comparison**

We compared the use of W-Re(26) and HT9 at a beam intensity of 2 mA and an outlet heat exchanger temperature of 180 ºC. In figure 4 we show the temperature and velocity fields in the LBE. We can observe that the funnel shape creates a recirculation zone in the downcomer end, which rises the coolant temperature before entering the funnel. This negative effect is compensated by the benefits obtained by the optimization of the flow in the spallation zone which is the most critical.

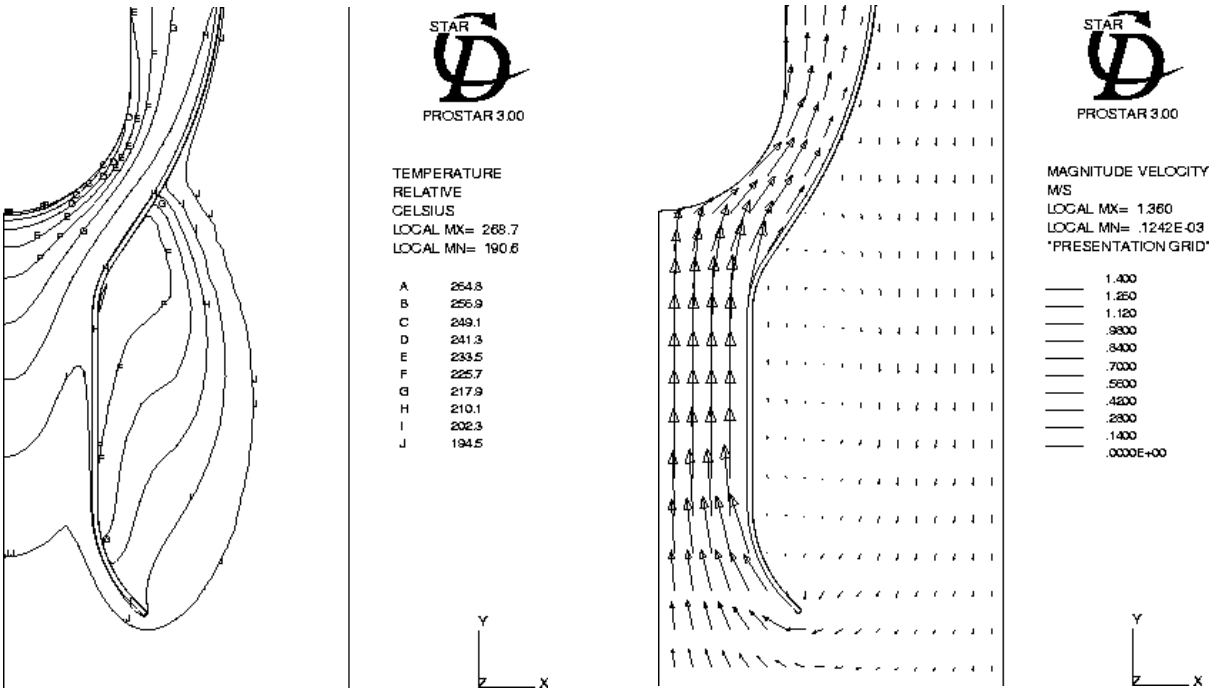


***Figure 4.*** *Temperature and velocity fields in the funnel region of the EAP target*

Temperature and velocity fields in the coolant are essentially independent on the beam window material: the main differences are only in the stresses induced in the window itself. In figure 5 we show the heat generated in the beam window in the two cases which is substantially different and depends essentially on the different densities of the two materials, which are shown in table 1. In spite of the fact that the power release in the window is about the double in the case of W-Re(26), temperatures are comparable, as shown in figure 5 and table 1, due to the much higher thermal conductivity of the Tungsten alloy.

| Material | Density ($Kg/cm^3$) | Thermal exp. coeff. ($1/10^6$ ºK) | Thermal conduct. ($W/m^oK$) | Heat release (kW) | Maximum Temperature (ºC) | Maximum Von Mises stress (MPa) |
|---|---|---|---|---|---|---|
| **W-Re(26)** | 19.7 | 4 | 140 | 13.4 | 322 | 334 (junction) |
| **HT9** | 7.7 | 9 | 24 | 7.2 | 319 | 50 (centre) |

***Table 1.*** *Window materials comparison*

The stress distribution in the window is quite similar for both cases except for the junction, which, in the case of heterogeneous materials, shows a stress peak which is comparable to the yield stress of HT9, as it is shown in

figure 6: the difference between the thermal expansion coefficients amplifies the bending effects due to the shearing forces involved in the connection of the cylinder with the hemispherical end. The junction between the window and the beam pipe in the case of heterogeneous materials, seems to be a very crucial problem not only for this reason, but also for the technological problems related to the welding technique.

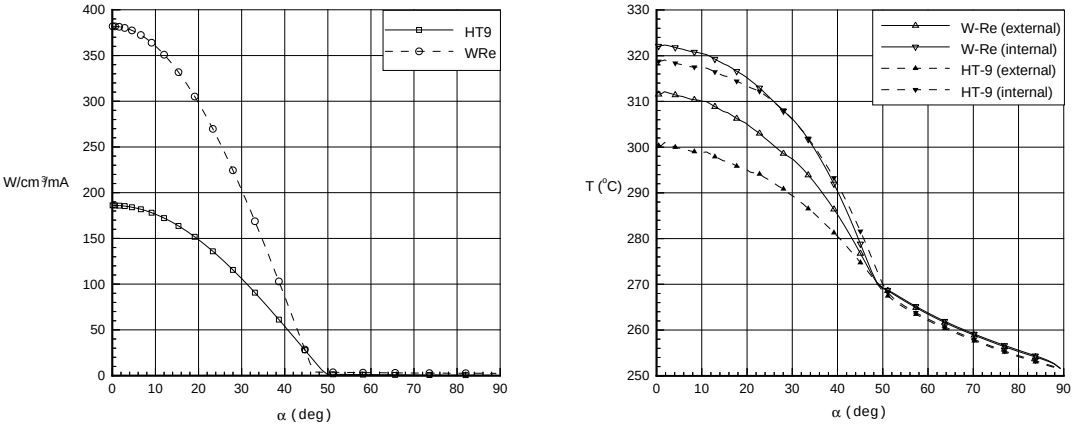


***Figure 5.*** *Power and Temperature distributions in the beam window*

We can also observe that the thinner part of the window, which is also the most loaded in the homogeneous case, undergoes strong bending moments depending basically on the temperature gradient along the thickness. The curves representing the stress components at the internal surface show a series of peaks in the proximity of the window centre. This behavior can be explained analytically by a superposition of oscillatory stress fields generated by the variation of the thickness.

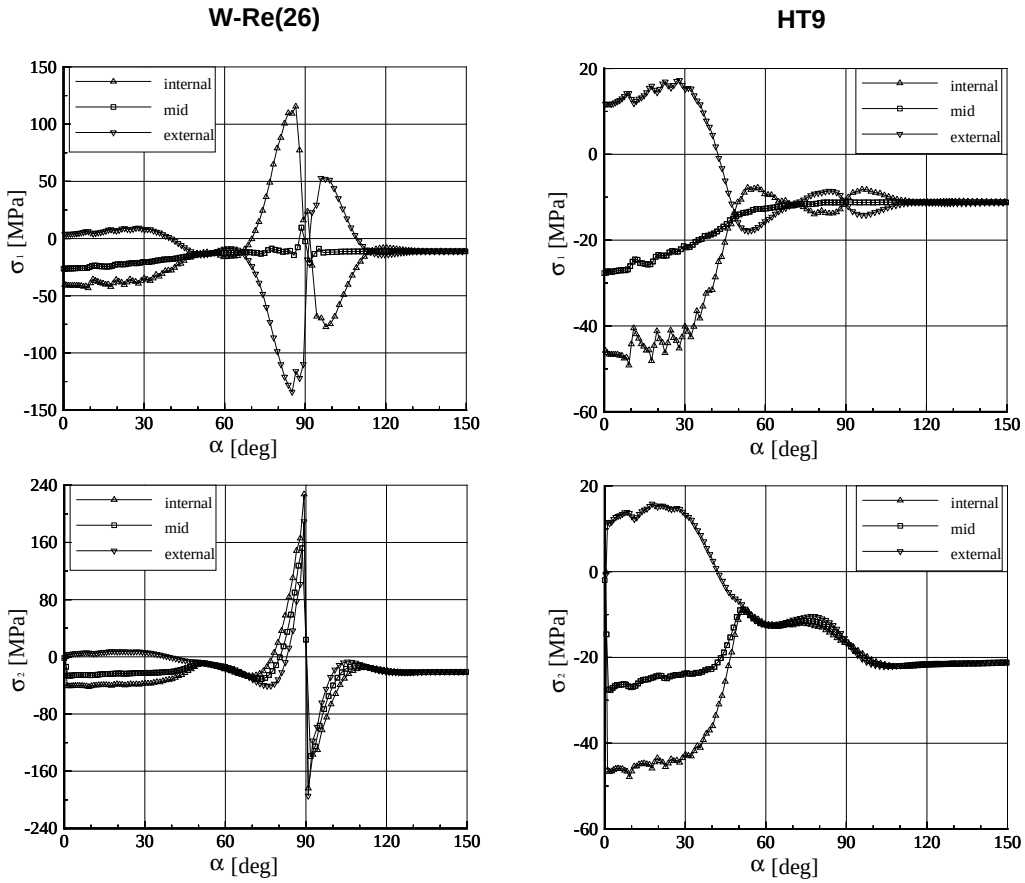

***Figure 6.*** *Meridional (σ1) and hoop (σ2) stress distribution at the external/middle/internal fibers of the window*

**Thermal Hydraulic optimization**

For the geometrical optimization we considered the pumping mechanism based on natural convection only. Given the external constraints in the geometry discussed before, the two most significant parameters to enhance the target performances are:

1. the funnel diameter $D_f$, which regulates the velocity of the coolant in the funnel (and therefore its temperature through the spallation region) and influences the heat exchange coefficient of the window.
2. the flow guide diameter $D_{fg}$, which acts on the pressure losses distribution in the coolant circuit and consequently on the mass flow rate).

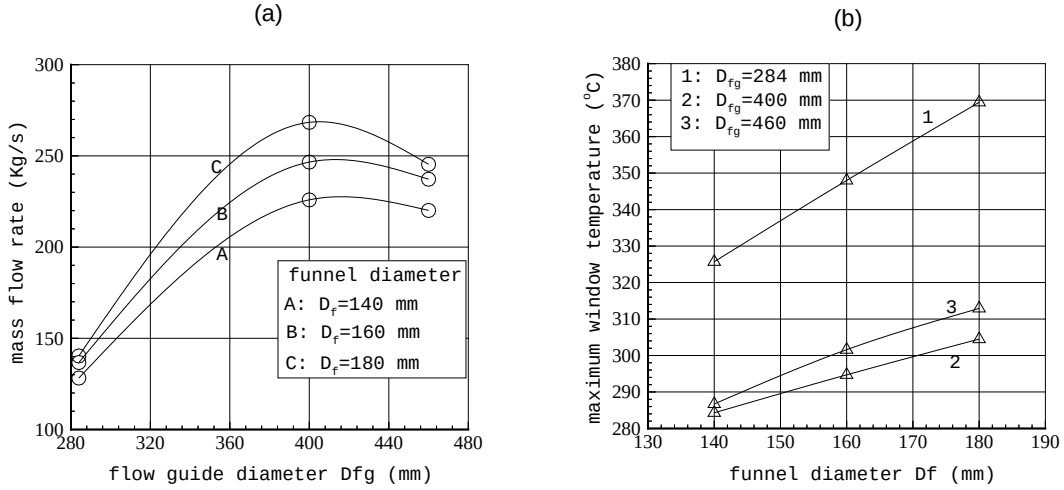


***Figure 7.*** *(a) Mass flow rate vs flow guide diameter for different funnel diameters. (b) Maximum window temperatures vs funnel diameter for different flow guide diameters.*

Figure 7 shows the dependence of the mass flow rate on the two parameters. For small values of $D_{fg}$ the pressure losses distributed in the rising column are much more important than the local losses in the inducer, the funnel and the connector, specially for larger values of $D_f$, so the mass flow rate is strongly dependent on $D_{fg}$. The maximum mass flow rate corresponds to $D_{fg}$ = 400 mm. However, although the mass flow rate decreases with $D_f$, the velocity in the funnel increases, leading to a lower heating of the coolant and hence to lower temperatures in the window itself.

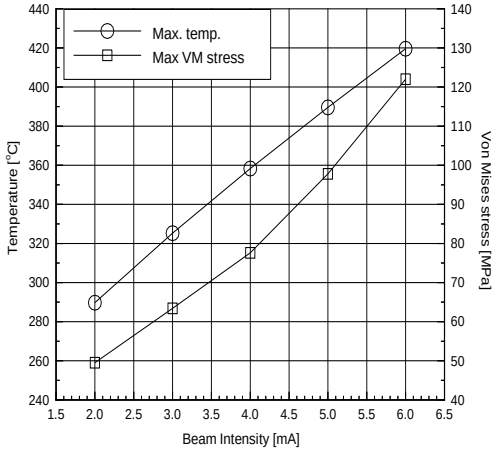


***Figure 8.*** *Maximum Temperatures and Von Mises stresses in the HT9 window vs beam intensity.*

**Beam intensity variations**

The beam intensity will change by a factor 3 during the fuel burnup. The effects of such variation on the maximum temperatures and Von Mises stresses in the window are reported in figure 8 for a case where the pumping mechanism is based on natural convection only.

Although the variation in temperatures and stresses is considerable, it is still in the working range of the HT9 steel. We notice that, although the maximum temperature can be lowered by enhancing the mass flow rate with an external pumping mechanism, the maximum stresses depend only on the beam intensity and distribution and very poorly on the cooling mechanism.

**Beam dimension variations**

One of the most dangerous accidents expected in the beam window is a reduction of the beam size. In order to analyze the effects of a variation of the beam size we reduced the beam spot diameter down to a dimension of 6 cm. Figure 9 shows that the maximum temperatures reached are immediately out of the utilization range of a ferritic steel.

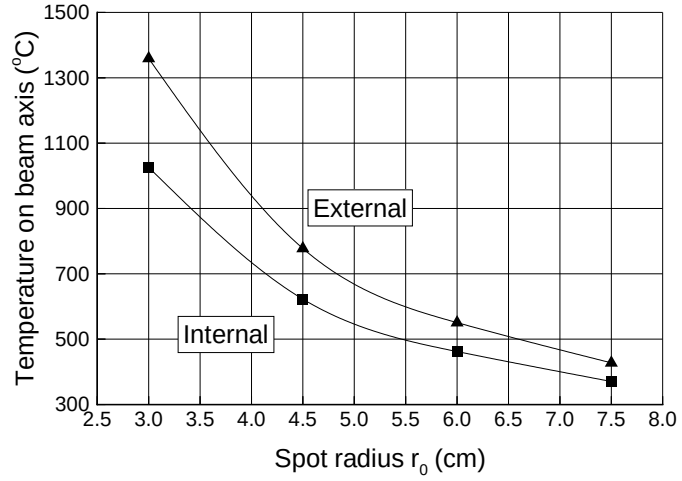


***Figure 9.*** *Maximum window temperatures vs beam radius.*

The same apply to the correspondent values of the stresses as it is shown in figure 10, where the maximum meridional, hoop and Von Mises stresses are shown as a function of the beam radius for a linear NASTRAN calculation.

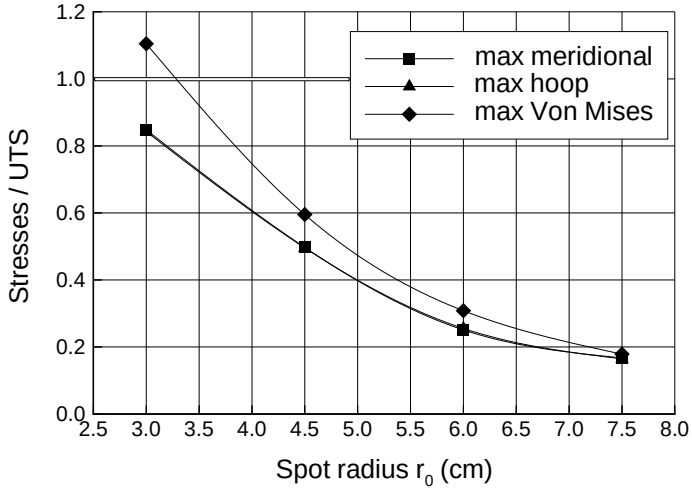


***Figure 10****. Maximum Meridional, hoop and Von Mises stresses normalized with UTS vs beam radius.*

## Conclusions

We illustrated the design of a Lead Bismuth Eutectic target for the Energy Amplifier 80 MW prototype. In the limits of the geometrical constraints of the system, a thermal hydraulic optimization of the target has been performed which allows the use of natural convection, eventually assisted by gas injection in the rising column, as the only pumping mechanism of the coolant.

The relatively low power beam of the machine allows the use of a ferritic steel (for example HT9) in the beam window, which deeply alleviates the problems related to the construction, the assembly and the operation of the window under intense proton irradiation, compared to a refractory material such as W-Re(26). Temperature and thermal stresses in the window/pipe system are largely in the working ranges of such steels.

## References


[1] *C. Rubbia et al.*, "Conceptual Design of a Fast Neutron Operated High Power Energy Amplifier", CERN Report, CERN/AT/95-44 (ET), Geneva, 29th September, 1995.
See also,
*C. Rubbia*, "A High Gain Energy Amplifier Operated with Fast Neutrons", AIP Conference Proceedings 346, International Conference on Accelerator-Driven Transmutation Technologies and Applications, Las Vegas, July 1994.

[2] Proceedings of the Meetings ICANS-XIII and ESS-PM4, edited by G. Bauer and R. Bercher, PSI proceedings 95-02, November 1995.

[3] Proceedings of the "International Workshop on the Technology and Thermal Hydraulics of Heavy Liquid Metals", compiled by B.R. Appleton and G.S. Bauer, Schruns, Montafon Valley, Austria, March 25-28 1996.

[4] *S. Andriamonje et al.* - Experimental determination of the energy generated in nuclear cascades by a high energy beam - Physics Letters B 348 (1995) 697-709.

[5] *A. FassÚ et al.*, "FLUKA92", Proc. of the Workshop on Simulating Accelerator Radiation Environments, Santa Fe, 11-15 January 1993
See also,
*A. Ferrari and P.R. Sala*, "Improvements to the Electromagnetic part of the FLUKA code", Proc. of the MC93 Int. Conf. on Monte-Carlo Simulation in High-Energy and Nuclear Physics, Tallahassee, 22-26 February 1993.

[6] *S. Buono, Y. Kadi, C. Rubbia* - Energy deposition of a Proton beam in the Lead target of the Energy Amplifier - CERN/ET Internal Note 97-11 (2 June 1997).

[7] *S. Buono, C. Rubbia* - A comparison of different materials for the beam window of the Energy Amplifier - CERN/ET Internal Note 96-26 (27 August 1996).

[8] *S. Buono, C. Rubbia* - A Tungsten-Rhenium Alloy as a beam window material for the Energy Amplifier - CERN/ET Internal Note 96-24 (9 July 1996).

[9] STAR-CD Version 3.05 User Guide, 1998 Computational Dynamics Limited.

[10] IDEAS Reference Manual, 1996, SDRC (Structural Dynamics Research Corporation)

[11] MSC/NASTRAN Reference Manual (Version 68), 1994, MacNeal-Schwendler Corporation